Journal of Alloys and Compounds 689 (2016) 161–168

Contents lists available at ScienceDirect

Journal of Alloys and Compounds

journal homepage: http://www.elsevier.com/locate/jalcom

Predictive Gibbs-energy approach to crystalline/amorphous relative stability of nanoparticles: Size-effect calculations and experimental test

J.L. Pelegrina [a, b, c, *], F.C. Gennari [a, b, c], A.M. Condó [a, b, c], A. Fernández Guillermet [a, b, c]

[a] Centro Atómico Bariloche, CNEA, R8402AGP, San Carlos de Bariloche, Argentina
[b] Instituto Balseiro, CNEA and Universidad Nacional de Cuyo, Argentina
[c] CONICET, Argentina

ARTICLE INFO

Article history:
Received 29 April 2016
Received in revised form
14 July 2016
Accepted 26 July 2016
Available online 29 July 2016

Keywords:
Nanoparticles
Mechanical alloying
Miedema model
Amorphous phase
Gibbs energy
Lattice-stability

ABSTRACT

Ball milling experiments performed in the last decade in various systems opened the question about the stability of crystalline nanoparticles with respect to the same group of atoms but in the amorphous state. The general purpose of the present work is to develop a predictive approach to this problem, and assess its accuracy by confronting thermodynamic calculations with experimental observations on Cu-Zn nanoparticles. The bases of the approach are as follows. First, the present Gibbs energy formalism makes use of the "lattice-stability" concept currently applied in so-called CALPHAD ("Calculation of Phase Diagrams") modeling work. Second, the enthalpy of formation of the alloy phases is treated in the framework of the Miedema model, with special attention to the parameters for the amorphous phase. Third, the surface contribution to Gibbs energy is accounted for. With the current thermodynamic description, the sizes of the crystalline nanoparticles which are stable with respect to the amorphous are determined by calculation. These predictions are confronted with the minimum size of the nanoparticles generated by subjecting γ-Cu-Zn powders to low-energy milling treatments, which is determined by X-ray diffraction and high-resolution transmission electron microscopy techniques. On this basis, a discussion is reported of the accuracy of the present approach. In particular, the parameters in the Gibbs energy description which crucially affect the agreement between calculations and experiments are highlighted.

1. Introduction

The current development of experimental methods to produce metallic nanoparticles has stimulated the theoretical interest in the thermodynamic account of the relative stability between the crystalline and amorphous phases in the nanoscale [1–4]. In principle, this problem should be treated in thermodynamic terms, by comparing the molar Gibbs energy (G_m) of the competing phases. However, the often limited equilibrium information on the crystalline phases, or the general lack of experimental data on the amorphous phases, makes it difficult to establish accurately the necessary G_m functions. As a consequence, there is a strong interest in the development of predictive methods to account for the stability of crystalline and amorphous nanoparticles, in particular, for alloys of practical interest.

Current attempts to produce G_m information on multicomponent alloy phases often make use of the so-called CALPHAD ("Calculation of Phase Diagrams") method [5,6]. This method aims at constructing phenomenological models for G_m of the various phases, and determining the parameters in the models by searching for the best fit ("optimization") to experimental phase-equilibrium and thermochemical data. The systematic application of this technique has shown that by combining the G_m functions for the binary subsystems, rather accurate predictions for the higher-order system properties might be obtained. On the other hand, when the binary experimental data are scarce, unreliable or lacking, the standard CALPHAD optimization method needs to be complemented by predictive approaches for thermodynamic properties.

The first purpose of the present work is the development of a

* Corresponding author. Centro Atómico Bariloche, CNEA, R8402AGP, San Carlos de Bariloche, Argentina.
E-mail address: jlp201@cab.cnea.gov.ar (J.L. Pelegrina).

http://dx.doi.org/10.1016/j.jallcom.2016.07.284
0925-8388/

predictive approach to crystalline/amorphous relative stability of metallic nanoparticles, which is consistent with the formulation of G_m currently adopted in CALPHAD modeling work. Specifically, when referring G_m of an alloy to that of the constituent elements, the structure differences will be accounted for in this work by using the concept of "lattice-stability" introduced by Kaufman [5]. For the usual structures of the elements, "lattice-stability" values have been presented [7], whereas the amorphous might be treated by relying either on specific approaches, such as that suggested by Loeff, Weeber and Miedema [8], or upon alternative, rather general assumptions on the amorphous state (Section 5). Once the reference states have been established, the various contributions to excess Gibbs energy of the competing phases will be treated in the framework of the Miedema approach [9] for the enthalpy of formation of alloys, by accounting for the structure effect upon the model parameters. In particular, the size-dependent surface contribution to G_m of these phases will be discussed in detail.

It should be emphasized that the Miedema model is currently the subject of a renewed interest in connection with the treatment of, in particular, the stability of amorphous phases and glasses [10–16] and the enthalpy of multicomponent, high-entropy liquid alloys [17–19]. In this context, the present work offers an alternative, enlightening way to test the predictive possibilities of the model.

The second purpose of the work is to assess the accuracy of the present approach by confronting its predictions with experimental data. The current methodology involves the thermodynamic prediction of the critical diameter (d_c^{ther}) of the crystalline nanoparticles which are stable with respect to the amorphous phase, and the comparison with the minimum diameter (d_{min}) of metallic nanoparticles obtained in ball milling experiments [20].

Specifically, the experimental part of the paper involves a study of the size-effect upon the stability of particles of the γ phase, a complex cubic phase [21] of the Cu-Zn system. To this aim, γ-Cu-Zn particles are generated through a mechanical milling treatment. This technique has previously been applied to the Cu-Zn system. In particular, high-energy ball milling techniques have previously been used to prepare alloys of various compositions starting from the elements [22–26]. Besides, exploratory mechanical-alloying (MA) studies for near equiatomic [22] and Zn-rich [23] compositions have also been reported. Moreover, Pabi et al. [24–26] studied the evolution of Cu-Zn phases with various compositions formed by MA, and related the phase stability to the particle sizes.

A particular motivation for the present experiments is the disagreement found between previous reports on the size effects upon the stability of nanoparticles in the Cu-Zn system [27,28]. In one such studies, low-energy milling experiments were performed upon a pre-alloyed equiatomic β_2 (CsCl-type structure) phase powder which induced a sharp reduction of the particle size [27]. Transmission electron microscopy (TEM) of the milled alloy indicated that crystalline particles with diameters of few nanometers were present, whereas X-ray diffraction (XRD) patterns suggested a mean particle-size about 50 times larger [27]. On the other hand, in Ref. [28] it was reported that the γ phase of a Cu_{35}-Zn_{65} alloy milled in a medium-energy apparatus is quite stable, and TEM observations showed that crystallite sizes decreased down to 20 nm, only. This result is unexpected because the γ structure is more brittle than β_2, and thus it was expected that the degree of fragmentation should be higher. In view of this striking discrepancy, new low-energy milling experiments of the γ phase have been performed in this work, to be compared with thermodynamic predictions.

2. Experimental procedures

A Cu - 61.67 at%Zn alloy (in the γ phase field) was prepared by melting commercial (99.99%) Cu and Zn in a sealed fused silica tube under Ar atmosphere in a resistance furnace. The resulting alloy was filed to obtain the starting powder for the mechanical milling process. The powder charge was of 10 g, without any process control agent, and seven bearing balls were added, resulting in a ball-to-powder weight ratio of about 47. An Ar atmosphere in the chamber with an overpressure of around 0.5 MPa was adopted. The mechanical milling was carried out at 177 rpm in an Uni-Ball-Mill II equipment (Australian Scientific Instruments), which is a low-energy milling device. It uses an external magnetic field to control the movement of the ferromagnetic steel balls that produce the milling inside a stainless steel container.

At specific milling times, 200 mg of powder was removed. The powder was scrapped from the walls when agglomeration and sticking effects were observed. Afterwards, the Ar atmosphere was reestablished. The structural and microstructural characteristics of the powders were analyzed by XRD in a Philips PW 1710/01 diffractometer using Cu Kα radiation and a graphite monochromator. The scans were recorded between 30° and 100° using a step of 0.02° and a counting time of 1 s.

The chemical composition of the milled powder was analyzed in a scanning electron microscope Philips SEM 515 using an EDAX energy dispersive spectrometer (EDS). TEM was performed using a Philips CM200 UT microscope operating at 200 kV, in either conventional imaging or high-resolution mode. Samples for TEM were prepared by dispersing a small amount of powder in ethanol, applying ultrasound during 900 s and depositing a drop of the resulting suspension on a commercial ultrathin carbon coated gold grid or lacey carbon coated copper grid.

3. Experimental results

The XRD pattern of the as-milled powder is shown in Fig. 1a. All the peaks can be consistently indexed with the structure of γ-Cu-Zn, indicating that the reduction in size of the powder did not favor the decomposition of the alloy. Determination of crystallite size and lattice strain was performed from the broadening of the XRD peaks, after subtracting the contribution of the instrument. A preliminary Hall–Williamson analysis indicated that microstrains were negligible in the powders. Therefore, crystallite sizes were calculated through the Scherrer equation. Crystallite size and lattice parameter (LP) of γ-Cu-Zn as a function of milling time is shown in Fig. 1b. An exponential decay (dashed line in Fig. 1b) has been associated with the evolution of the size of the diffracting domains, from which a time constant of 15 h has been determined. From the least-squares fit a mean value of (11 ± 1) nm for the final crystallite size was established. Furthermore, taking into consideration the experimental scatter, it can be stated that the LP shows a negligible variation with milling time. The mean LP, as determined from Fig. 1b, is (0.888 ± 0.001) nm.

The chemical analysis conducted in the scanning electron microscope by examining the as milled powder in several points was consistent with the nominal composition of the alloy. Only traces of Fe and Cr, the main constituents of the milling environment, were found as contamination. The samples for TEM showed an agglomeration of crystallites, as can be seen in Fig. 2a. The corresponding selected area electron diffraction pattern, shown in Fig. 2a inset, can be consistently indexed as that corresponding to the γ phase. Crystallite sizes were obtained from a dark field image of the zone, which is shown in Fig. 2b. The particles highlighted with a white square have a diameter of (9 ± 1) nm. The EDS analysis of the crystallites, shown in Fig. 3a, yielded a value of Cu - 60 at%Zn, in reasonable agreement with the nominal composition. A high-resolution TEM image of one crystallite protruding out of one border of the agglomerate is shown in Fig. 3b. The size of the

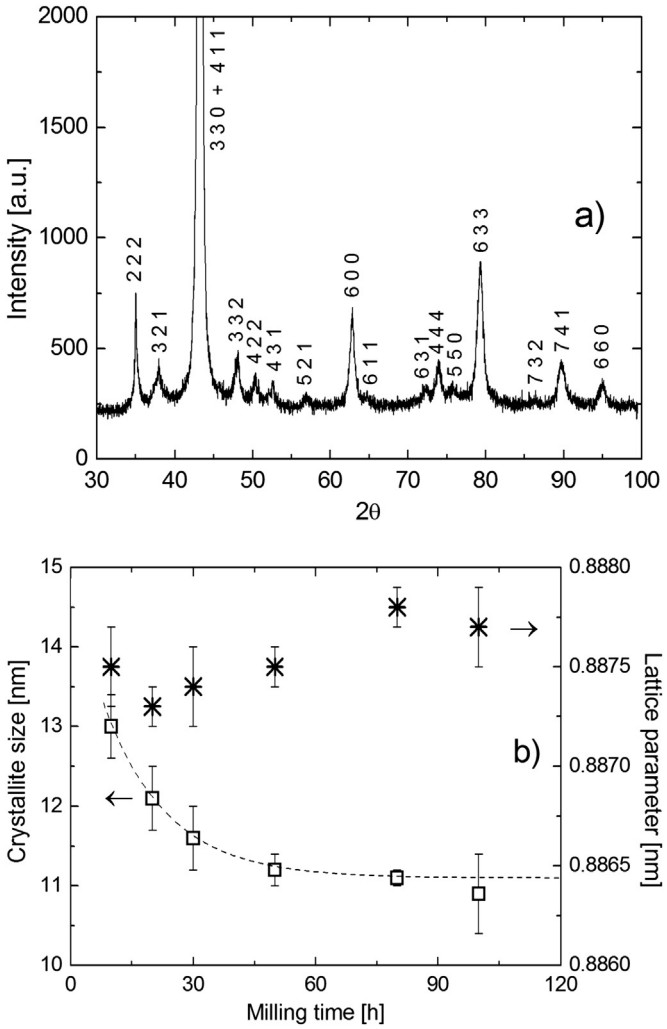

Fig. 1. a) XRD pattern of γ-Cu-Zn milled for 60 h. b) Crystallite size and lattice parameter of γ-Cu-Zn as a function of milling time.

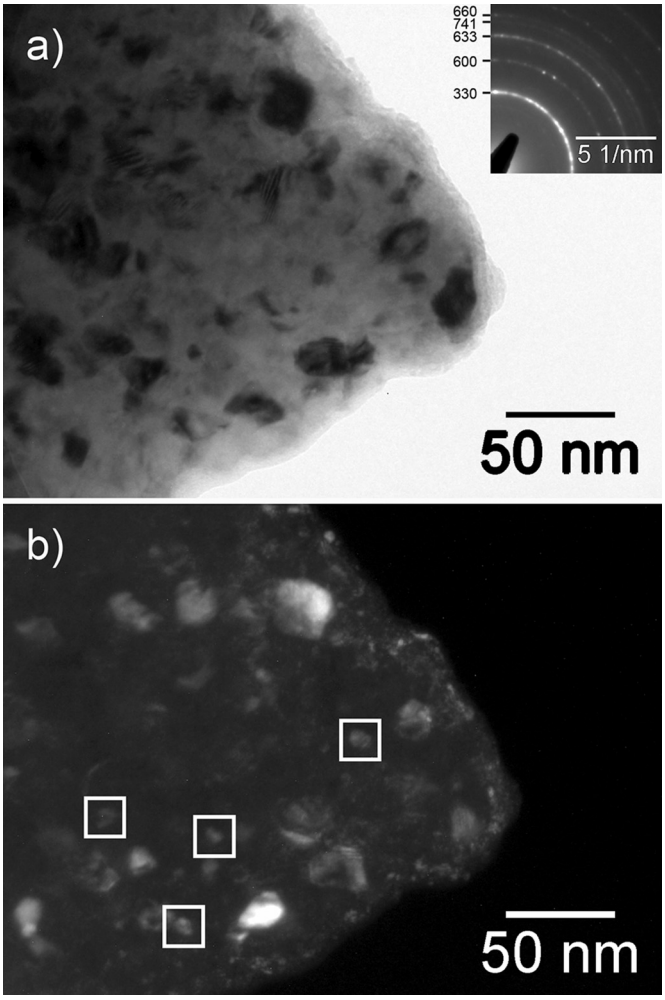

Fig. 2. Agglomerate of γ phase crystallites. a) Bright field TEM micrograph and corresponding electron diffraction pattern (inset). b) Dark-field image using an inner diffraction ring. The smaller crystallites are indicated by white squares.

crystallite is around 9 nm and the orientation, obtained by performing the Fast Fourier Transform of the image, corresponds to the [3 2 5] zone axis of the γ structure (Fig. 3b inset). It is to be remarked that the difference between the particle sizes determined by XRD and by TEM is not as high as that reported for the β_2 phase [27].

The key finding of the experimental part is that any possible crystalline-to-amorphous transition can only take place for γ phase nanoparticles smaller than 9 nm, instead of the 20 nm limit reported in Ref. [28]. The presently determined d_{min} will, therefore, be adopted in the remaining of the paper as an upper limit of the acceptable values for the thermodynamically predicted d_c^{ther}, i.e.

$$d_c^{ther} \leq d_{min} = (9\pm1)\ nm \tag{1}$$

4. Gibbs energy formalism

The molar Gibbs energy (G^θ) of a substitutional A-B crystalline ("c") or amorphous ("a") phase θ (θ = c, a) at a given temperature (T) and pressure will be expressed as

$$G^\theta = X_A\ {}^0G_A^\theta + X_B\ {}^0G_B^\theta + \Delta H^\theta - T\Delta S^\theta + \Delta G^{\gamma,\theta} \tag{2}$$

where X_i is the mol fraction and ${}^0G_i^\theta$ is the Gibbs energy per mole of the element "i" (i = A, B) in the phase θ, ΔH^θ and ΔS^θ are respectively the enthalpy and the entropy of formation of the phase, and $\Delta G^{\gamma,\theta}$ is the surface contribution to Gibbs energy of θ. In the present work the focus is on ΔG^θ, the Gibbs energy formation of the phase, with respect to the elements A and B in their stable ("st") structure, at the given temperature and pressure, which is obtained from eq. (2) as

$$\begin{aligned}\Delta G^\theta &= G^\theta - X_A\ {}^0G_A^{st} - X_B\ {}^0G_B^{st} \\ &= X_A\ \Delta^0G_A^{\theta/st} + X_B\ \Delta^0G_B^{\theta/st} + \Delta H^\theta - T\ \Delta S^\theta + \Delta G^{\gamma,\theta}\end{aligned} \tag{3}$$

where $\Delta^0G_i^{\theta/st} = {}^0G_i^\theta - {}^0G_i^{st}$ (i = A, B) are the "lattice stabilities" of the elements [5].

4.1. Enthalpy of formation

4.1.1. General expressions

By adopting the Miedema approach, the ΔH^θ term in eq. (3) with θ = c or a, will be expressed as the sum of a chemical ("chem"), elastic ("elas") and structural ("stru") contribution [29], as follows

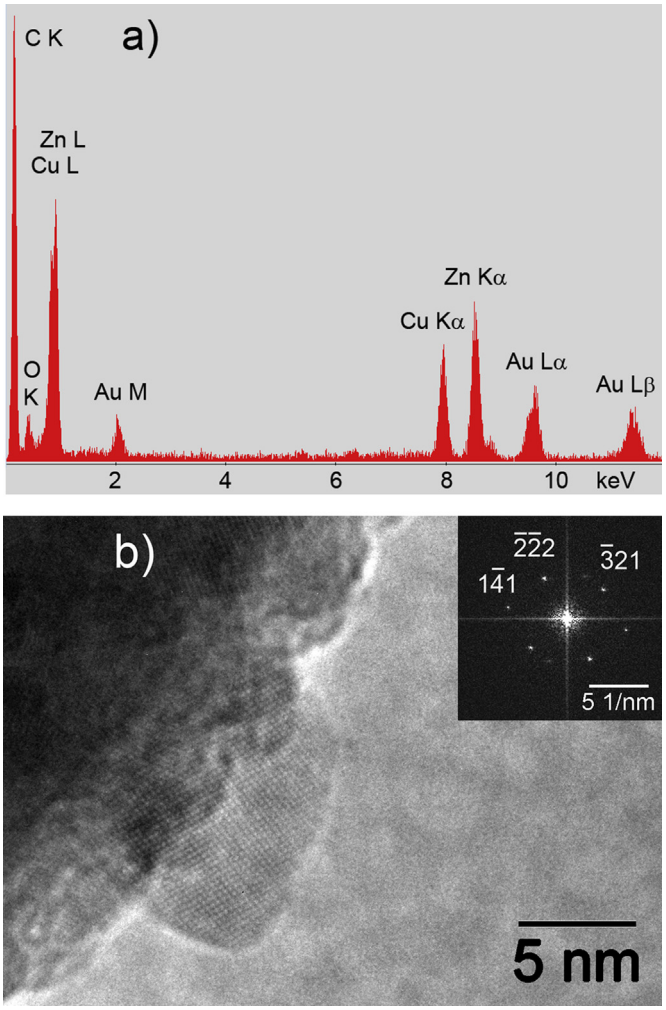

Fig. 3. a) EDS spectrum corresponding to the γ phase Cu-Zn crystallites on an ultrathin carbon-coated gold grid. b) High-resolution TEM micrograph of a protruding particle oriented in the [3 2 5] zone axis, as indicated in the Fast Fourier Transform of the image (inset).

$$\Delta H^{\theta} = \Delta H^{\theta}_{chem} + \Delta H^{\theta}_{elas} + \Delta H^{\theta}_{stru} \tag{4}$$

The first contribution in eq. (4) is given by the Miedema model as the weighted average of the solution enthalpies of one element into the other, i.e.,

$$\Delta H^{\theta}_{chem} = X_A\, X_B \left(f^A_B\, \Delta H^{A\ in\ B}_{sol} + f^B_A\, \Delta H^{B\ in\ A}_{sol} \right) \tag{5}$$

where the coefficients

$$f^i_j = C^{\theta}_j \left[1 + k^{\theta} \left(C^{\theta}_i\, C^{\theta}_j \right)^2 \right] \tag{6}$$

represent the degree by which a "j" atom is surrounded by an "i" atom, and are calculated from the surface concentration C^{θ}_j of the "j" atoms as $C^{\theta}_j = \frac{X_j\,(V^{\theta}_j)^{2/3}}{X_j\,(V^{\theta}_j)^{2/3} + X_i\,(V^{\theta}_i)^{2/3}}$ using the molar volumes V^{θ}_i of the elements.

The k^{θ} parameter in eq. (6) was introduced by Miedema in order to account phenomenologically for the effect of the degree of ordering of the phase upon the contact area between dissimilar atoms. Three characteristic values have been generally adopted in the literature. Disordered phases (both crystalline and amorphous) were described with $k^{\theta} = 0$ [28,30]; short-range ordered alloys (both crystalline and amorphous) with $k^{\theta} = 5$ [16,30,31], and long-range ordered alloys and intermetallic compounds with $k^{\theta} = 8$ [28,30,31]. The k^{θ} values adopted in the present work are discussed in the next subsection.

The solution enthalpy in eq. (5) is calculated by using the relation

$$\Delta H^{i\ in\ j}_{sol} = \left[\frac{\left(V^{\theta}_i\right)^{2/3}}{\left(n^{-1/3}_{WS}\right)_{av}} \right] \left[-P^{\theta}\,(\Delta\Phi)^2 + Q^{\theta} \left(\Delta n^{1/3}_{WS}\right)^2 - R^{\theta} \right] \tag{7}$$

where $n_{WS,i}$ is the electron density at the boundary of the Wigner-Seitz cell of the element "i", P^{θ}, Q^{θ} and R^{θ} represent empirical constants, and Φ the work function. The symbol "Δ" stands for the difference and the subscript "av" for the arithmetical mean value. With the volume expressed in cm^3/mol, the work function Φ in volts and the electron density n_{WS} in cm^{-3} the enthalpy is obtained in J/mol.

The second term in eq. (4) is due to the different sizes of the atoms that occupy equivalent lattice positions. It is expressed as the weighted average of the elastic mismatch energies [32].

$$\Delta H^{\theta}_{elas} = X_A\, X_B \left(f^A_B\, \Delta E^{A\ in\ B}_{elas} + f^B_A\, \Delta E^{B\ in\ A}_{elas} \right) \tag{8}$$

with

$$\Delta E^{i\ in\ j}_{elas} = \frac{2\,K^{\theta}_i\,\mu^{\theta}_j \left(V^{\theta}_j - V^{\theta}_i\right)^2}{3\,K^{\theta}_i\,V^{\theta}_j + 4\,\mu^{\theta}_j\,V^{\theta}_i} \tag{9}$$

where K^{θ}_i and μ^{θ}_i are the bulk and the shear modulus of the "i" element in the phase θ, respectively.

The third term in eq. (4) has been considered to be much smaller than the other two for alloys of a noble metal with an hcp transition metal [8]. Therefore this term will be neglected in the present calculations.

4.1.2. Application to the present crystalline and amorphous phases

For the crystalline phase ($\theta = c$), ΔH^c was obtained from eqs. (4), (5) and (8) with the proper parameters. In particular, the values $P^c = 12300$, $Q^c = 115620$ and $R^c = 5170$ suggested in Ref. [33] were adopted. Concerning the "k" parameter in eq. (6), it should be mentioned that equiatomic Cu-Zn alloys are prone to develop long-range ordered structures [34] and also that the present γ-Cu-Zn alloy has ordered structural vacancies [35]. On these bases the value $k^c = 8$ was accepted in the present calculations.

For the amorphous phase ($\theta = a$) an expression similar to eq. (4) will be adopted. However, as suggested by Loeff, Weeber and Miedema [8], in this case the ΔH^a_{elas} contribution might be strongly reduced. Such approximation will be accepted, and thus the ΔH^a_{elas} term will be neglected in the present work, i.e., the enthalpy of formation of the amorphous phase will be calculated as

$$\Delta H^a = \Delta H^a_{chem} \tag{10}$$

and this chemical contribution will be evaluated using eqs. (5)–(7). In eq. (7) the same P^a and Q^a parameters as for the crystal were used, whereas $R^a = 3770$ given in Ref. [33] for the liquid phase, were accepted. The latter choice is in line with the present consideration of the amorphous as an undercooled liquid (Section 5). In eq. (6) the value $k^a = 5$ usually adopted for amorphous phases [16] was used in this work.

Other parameters for the elements Cu and Zn used in the

calculations are listed in Table 1.

4.2. Entropy of formation

The entropy of formation of the phase θ will be expressed as

$$\Delta S^{\theta} = \Delta S^{\theta,id} + {}^{E}S^{\theta} = -R_G\,(X_A\,lnX_A + X_B\,lnX_B) + {}^{E}S^{\theta} \tag{11}$$

where R_G is the gas constant. The first term ($\Delta S^{\theta,id}$) represents the entropy of mixing of an ideal solution and the excess entropy term (${}^{E}S^{\theta}$) accounts for the deviations from the ideal model. Equation (11) was used to describe the entropy of formation of both the crystalline and the amorphous phase. As a first approximation, the relation ${}^{E}S^{c} = {}^{E}S^{a}$ was adopted. This simplification implies that the possible effects upon the excess entropy term of the difference in the degree of ordering between the crystal and the amorphous is neglected.

4.3. The $\Delta G^{\gamma,\theta}$ contribution

The key quantity to be compared with the low-energy milling experiments is the Gibbs energy difference between a crystalline spherical particle and the same particle in the amorphous state. The proper evaluation of the surface contribution to Gibbs energy ($\Delta G^{\gamma,\theta}$) has been a subject of recent discussion. Often, the so-called Kelvin formulation, based on the curvature of the surface, has been used. However, Kaptay [38,39] has pointed out that the Gibbs formulation, involving the specific area of the particle, should be preferred. Accordingly, in the present work the last term in eq. (2) is expressed as

$$\Delta G^{\gamma,\theta} = \left(\frac{\Sigma}{\Omega}\right)\gamma^{\theta}\,V^{\theta} = \left(\frac{6}{d}\right)\gamma^{\theta}\,V^{\theta} \tag{12}$$

where γ^{θ} (θ = c, a) is the surface energy per unit area of the material, $\Sigma = \pi\,d^2$ the surface, $\Omega = \pi\,\frac{d^3}{6}$ the volume and d is the diameter of the spherical particles.

Equation (12) was applied assuming that both phases have the same shape, viz. spherical. In this equation the γ^{θ} parameter for the amorphous and the crystalline phase is a temperature and composition dependent quantity. Furthermore, the γ^{θ} parameters are assumed to depend upon the curvature of the particle. This problem is the subject of an extensive literature, and various alternative equations have been presented to account for the effect of the diameter d of the particle upon γ^{θ} [38]. In particular, the equations by Tolman and Vogelsberger yield, respectively, the highest and lowest surface energy corrections. Both equations [38,40], viz.,

$$\gamma^{\theta} = \left(\frac{d}{d + 4\,\delta^{\theta}}\right)\gamma^{\theta}_{\infty} \tag{13}$$

and

$$\gamma^{\theta} = \left(1 - \frac{4\,\delta^{\theta}}{d}\right)\gamma^{\theta}_{\infty} \tag{14}$$

were tested. In eqs. (13) and (14), the surface energy parameter γ^{θ}_{∞} is a temperature- and composition-dependent quantity which is assessed in the next section, and δ^{θ}, the so-called Tolman parameter, characterizes the width of the interface [40]. In the present work, lacking more specific information, the Tolman parameter was estimated for both phases as one half of the spacing between the closest-packed planes in the crystalline phase. Using the lattice parameter value reported in Section 3, this approximation yields $\delta^{\theta} = 0.1\ nm$ ($\theta = c,a$).

5. "Lattice-stability" and surface energy contributions

5.1. "Lattice-stability" of Cu and Zn in the crystalline and amorphous phases

For the fcc, bcc and hcp phases of the elements Cu and Zn, the differences $\Delta^0 G_i^{\theta/st} = {}^0G_i^{\theta} - {}^0G_i^{st}$ were taken directly from the literature [7]. The structure of the γ phase can be described by the arrangement of 3 × 3 × 3 body centered cubic cells, having 52 atoms in this complex cubic structure and two structural vacancies, one at the center and another at the vertices of the cube [41]. As a first approximation this phase was treated as a bcc phase and the differences $\Delta^0 G_i^{c/st} = {}^0G_i^{c} - {}^0G_i^{st}$ were evaluated at $T = 300\ K$ using the bcc/fcc and bcc/hcp Gibbs energy differences presented in Ref. [7], i.e.,

$$\Delta^0 G_{Cu}^{bcc/fcc} = 3641\ \frac{J}{mol}\ \text{and}\ \Delta^0 G_{zn}^{bcc/hcp} = 2134\,\frac{J}{mol} \tag{15}$$

The $\Delta^0 G_i^{a/st} = {}^0G_i^{a} - {}^0G_i^{st}$ differences corresponding to Cu and Zn in the amorphous phase are not available. In view of this problem, three estimation methods based on comparing the amorphous with an undercooled liquid ("liq") were tested, as follows.

A first possibility is to directly identify the amorphous phase with the undercooled liquid and assume

$$\Delta^0 G_i^{a/st} = \Delta^0 G_i^{liq/st} \tag{16}$$

and similarly for $\Delta^0 H_i^{a/st}$ and $\Delta^0 S_i^{a/st}$. However, when applying eq. (16), the low-temperature values for $\Delta^0 G_i^{a/st}$ may be obtained in different ways. The simplest alternative, referred to in the following as "Method I" involves an extrapolation of the usually linear $\Delta^0 G_i^{liq/st}$ vs. T relations based on information on the stable liquid phase at high temperatures, such as those presented in Ref. [7].

Alternatively, when extrapolating the properties of the liquid phase to low temperatures, Fernández Guillermet and Hillert [42] accepted the general belief that: i) there will be a glass-transition at about one third of the melting temperature (T_m), and below that point the heat capacity of the liquid will be similar to that of the crystalline phase; and, ii) the entropy of the liquid is more or less approaching that of the crystalline phase at the glass transition. Accepting these concepts they arrived [42] at an extrapolated $\Delta^0 G_i^{liq/st}$ vs. T relation which becomes approximately horizontal for temperatures below (1/3) T_m. If the amorphous phase is identified with such undercooled liquid, for temperatures $0<T<(1/3)\ T_m$ the

Table 1
Values of the parameters of the Miedema model for Cu and Zn adopted in the present work.

	V^c [cm^3/mol]	V^{liq} [cm^3/mol]	Φ [V]	$n_{WS}^{1/3}$ [cm^{-1}]	T_m [K]	K^c [GPa]	μ^c [GPa]	γ^c_{∞} [J m^{-2}]	γ^{liq}_{∞} [J m^{-2}]
Ref.	[9]	[36]	[9]	[9]	[37]	[28]	[28]	[9]	[36]
Cu	7.117	7.416	4.45	1.47	1358	140	48	1.825	1.285
Zn	9.167	9.598	4.10	1.32	693	70	43	0.990	0.782

results in Ref. [42] imply that

$$\Delta^0 G_i^{a/st}(T) = \Delta^0 G_i^{liq/st}(T_m/3) \quad (17)$$

This extrapolation method will be referred to in the following as "Method II".

Finally, Loeff, Weeber and Miedema [8] focused directly on the enthalpy of the amorphous phase, suggesting that

$$\Delta^0 H_i^{a/st} < \Delta^0 H_i^{liq/st}(T_m) \quad (18)$$

Their estimation method is based on expressing $\Delta^0 H_i^{a/st}$ as proportional to T_m with a proportionality coefficient that is smaller than the usual entropy of melting of the elements [8], viz.,

$$\Delta^0 H_i^{a/st} = 3.5\, T_{m,i} \quad (\mathrm{i} = \mathrm{Cu},\ \mathrm{Zn}) \quad (19)$$

In this way they tried to account for a possible relaxation of the amorphous towards the crystalline state. In the present work eq. (19) was used to estimate the $\Delta^0 G_i^{a/st}$ differences for Cu and Zn, by further assuming that $\Delta^0 S_i^{a/st}$ is negligible at 300 K. This procedure, will be referred to as "Method III".

The $\Delta^0 G_i^{a/st}$ values obtained by applying the three estimation procedures at $T = 300\ K$ are listed in Table 2. The $X_{Cu}\ \Delta^0 G_{cu}^{a/st} + X_{Zn}\ \Delta^0 G_{zn}^{a/st}$ vs. composition relations based on these values are presented in Fig. 4. It is found that the treatment of the amorphous phase as an undercooled liquid (Method I and Method II) leads to the highest values, whereas Method III [8] yields the lowest ones.

5.2. Surface Gibbs energy parameters

Direct measurements of the γ_∞^θ parameter for the present alloy in both the crystalline and amorphous states were not found in the literature. As a consequence, estimation methods were developed which make use of experimental data available on Cu and Zn and relies upon current generalizations about the composition dependence of γ_∞^θ for alloys. As stated before, γ_∞^a was identified with the γ_∞^{liq} parameter corresponding to a liquid phase undercooled down to 300 K.

5.2.1. Database with γ_∞^θ for solid and liquid phases of the elements

The $\gamma_{\infty,i}^c$ parameters for i = Cu, Zn were taken from the work by Miedema [43]. His values, corresponding to $T = 0\ K$ were corrected to 300 K by assuming linear temperature dependences, and the (negative) $(\partial\gamma_{\infty,i}^c/\partial T)$ quantities recommended in the same paper [43]. The $\gamma_{\infty,i}^{liq}$ for Cu and Zn were taken from Ref. [36]. The recommended values, corresponding to measurements at high temperatures, were corrected to 300 K by assuming linear temperature dependencies, and the respective (negative) $(\partial\gamma_{\infty,i}^{liq}/\partial T)$ quantities recommended in the same table [36].

In order to apply the estimation methods for the composition dependence of the surface energy parameter of the alloy $(\gamma_{\infty,CuZn}^\theta)$ (see below), high-temperature values of $\gamma_{\infty,i}^{liq}(T_m)$ and low-temperature values $\gamma_{\infty,i}^c(0\,K)$ were obtained from the quoted sources [36,43] for various elements with similar values of the electron-density parameter $n_{WS,i}$(in parentheses), viz., Ag (2.515), Al (2.686), Cd (1.907), Cu (3.177), Ga (2.248), In (1.602) and Zn (2.300) [9]. The selected values for $\gamma_{\infty,i}^c$ and $\gamma_{\infty,i}^{liq}$ are plotted in Fig. 5a using squares and circles, respectively. The solid lines represent second-degree least-squares fits. The smooth variations of the γ_∞^θ with n_{WS} encourages an interpolation for the present Cu-Zn alloy (Section 5.2.2.). With this aim, the $\gamma_{\infty,i}^c$ and $\gamma_{\infty,i}^{liq}$ data in Fig. 5a were corrected to 300 K by using the temperature dependencies recommended in Refs. [36,43] respectively, and fitted to second-degree polynomials. The results of the fit are plotted in Fig. 5b.

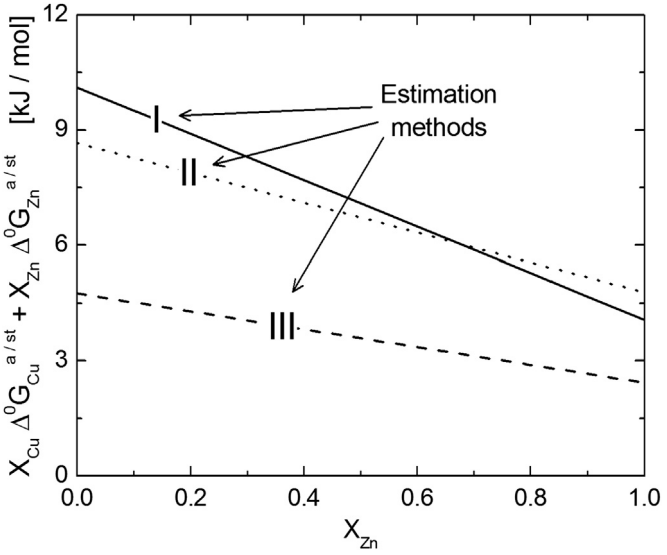

Fig. 4. The sum of the first two terms in eq. (3) for the amorphous phase as a function of Zn concentration. The roman numbers refer to the particular method used to estimate the energy of the amorphous phase (see text for details).

5.2.2. Estimation of the $\gamma_{\infty,CuZn}^\theta$ parameters for the Cu - 61.67 at%Zn alloy

The composition dependence of γ_∞^θ parameters has been discussed in the literature in terms of thermodynamic models involving the excess Gibbs energy of the components and their segregation to the surface [44–46]. However, those approaches involve thermodynamic information which unfortunately is not available for the present alloys. As a consequence, two interpolation procedures which are related to the present theoretical framework, will be applied in the following.

The first procedure makes use of an equation derived by Benedictus, Böttger and Mittemeijer [47] on the basis of the Miedema model, viz.,

$$\gamma_{\infty,CuZn}^\theta = C_{Cu}^\theta\ \gamma_{\infty,Cu}^\theta + C_{Zn}^\theta\ \gamma_{\infty,Zn}^\theta - \frac{C_{Cu}^\theta\ C_{Zn}^\theta}{C_0}\ \frac{\Delta H_{sol}^{Cu\ in\ Zn}}{\left(V_{Cu}^\theta\right)^{2/3}} \quad (20)$$

where C_0 is a constant depending on the shape of the Wigner-Seitz cell. According to [9], $C_0 = 4.5\ x\ 10^8$.

The second interpolation procedure relies upon the empirical correlation between γ_∞^θ and n_{WS} for elements early discussed by

Table 2
Estimated $\Delta^0 G_i^{a/st}$ values for Cu and Zn.

Method	Estimation based on	$\Delta^0 G_{cu}^{a/fcc}$ [J/mol]	$\Delta^0 G_{Zn}^{a/hcp}$ [J/mol]
I	Linear extrapolation [7]	10112	4069
II	Approximate account of the glass transition [42]	8660	4780
III	Loeff et al. [8]	4753	2426

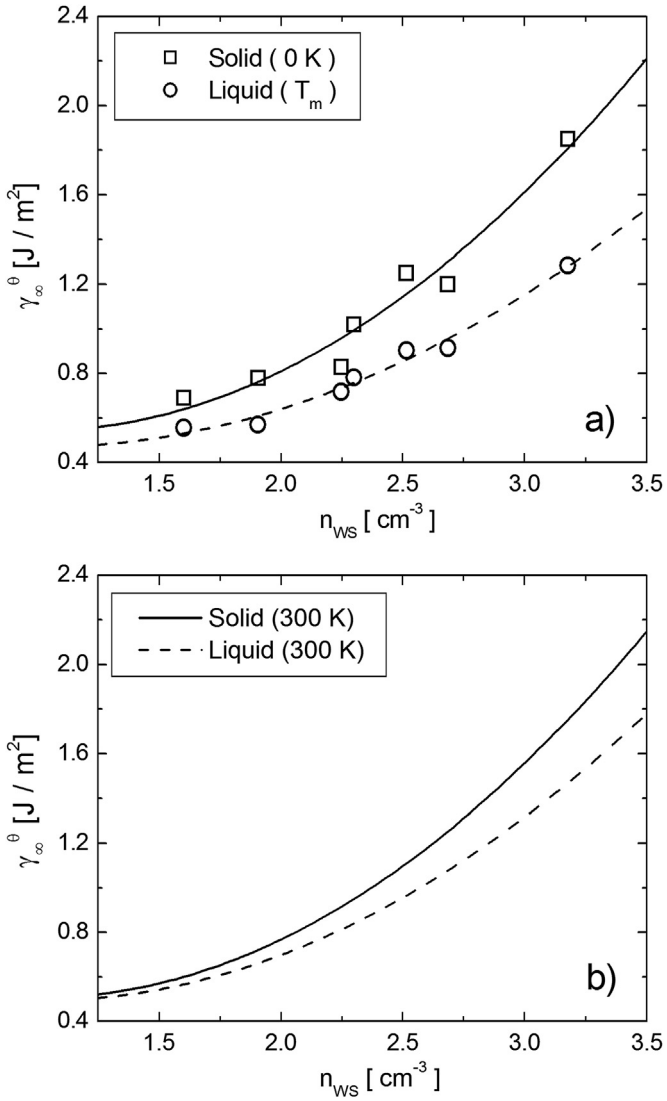

Fig. 5. Surface energy parameter as a function of the electron density. a) Selected values for pure elements at 0 K for the crystal and at the melting temperature for the liquid, with the corresponding parabolic least-squares fits. b) Second-degree least-squares fits to the data of the pure elements corrected to room temperature.

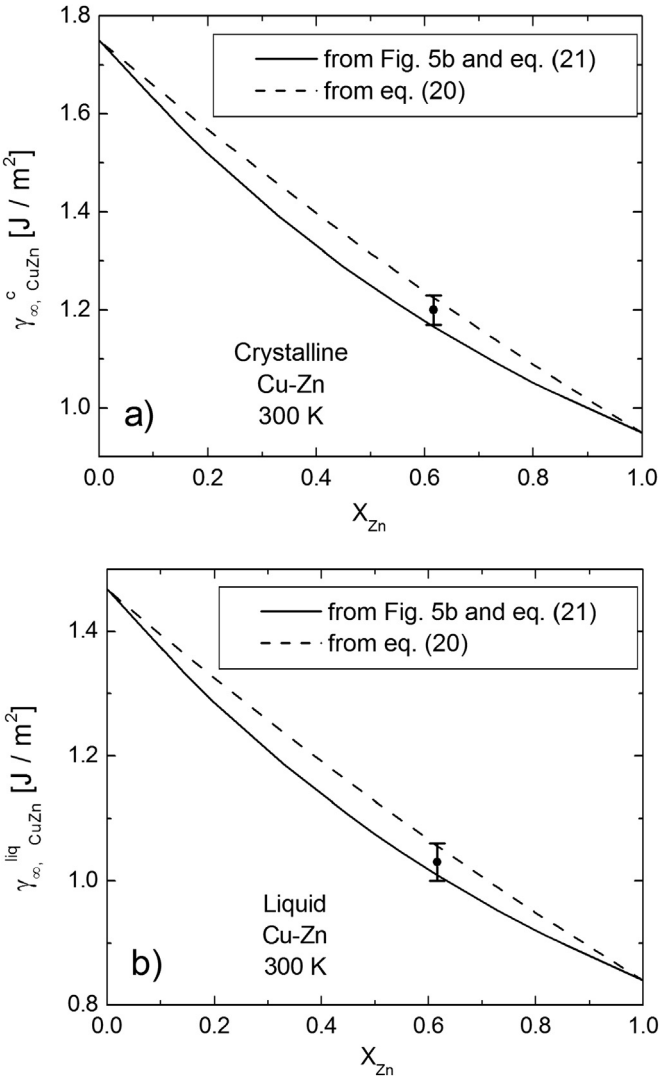

Fig. 6. Surface energy parameter as a function of composition for a) the crystal and b) the liquid Cu-Zn alloys. The filled circles with error bars represent present estimates (see text for details).

Miedema and coworkers [9] and demonstrated in Fig. 5. In the present work these ideas were adopted to estimate $\gamma^c_{\infty,CuZn}$ and $\gamma^{liq}_{\infty,CuZn}$ by interpolating the values in Fig. 5b. To this end, the $n^c_{WS,CuZn}$ and $n^{liq}_{WS,CuZn}$ parameters for the Cu - 61.67 at%Zn liquid and crystalline alloys were evaluated using the following expression, which has previously been applied to binary and ternary alloys and intermetallic compounds [48].

$$n^\theta_{WS,CuZn} = \frac{X_{Cu}\, V^\theta_{Cu}\, n_{WS,Cu} + X_{Zn}\, V^\theta_{Zn}\, n_{WS,Zn}}{X_{Cu}\, V^\theta_{Cu} + X_{Zn}\, V^\theta_{Zn}} \tag{21}$$

The composition dependence of the $\gamma^c_{\infty,CuZn}$ and $\gamma^{liq}_{\infty,CuZn}$ parameters for Cu-Zn alloys obtained by applying both interpolation procedures are plotted using solid lines in Fig. 6a and b, respectively. The filled symbols with error bars represent the present estimates for the crystalline and amorphous Cu - 61.67 at%Zn alloys, viz., $\gamma^c_{\infty,CuZn} = (1.20\pm0.03)\ J/m^2$ and $\gamma^{liq}_{\infty,CuZn} = (1.03\pm0.03)\ J/m^2$. These estimates are in line with two main generalizations about the surface energy data, reported by Chatain [49], viz., i) the composition dependence of the γ^θ_∞ parameters for alloys is non-linear; and ii) the $\gamma^c_\infty/\gamma^{liq}_\infty$ ratio for alloys falls in the range 1.15–1.20. The present value (1.155) matches this general trend.

In view of these facts, the estimated $\gamma^c_{\infty,CuZn}$ and $\gamma^a_{\infty,CuZn} = \gamma^{liq}_{\infty,CuZn}$ values were inserted in eqs. (13) and (14), to model the surface contribution to Gibbs energy.

6. Discussion of critical diameters and concluding remarks

The critical diameter d^{ther}_c for crystalline/amorphous relative stability was obtained from the present formalism (Eq. (3)) by making

$$\Delta G^a = \Delta G^c \tag{22}$$

at T = 300 K, for each of the amorphous lattice-stability estimation methods I, II and III, and the results of Tolman and Vogelsberger equations for γ^θ. The d^{ther}_c values obtained in this way are listed in Table 3. For each of the amorphous lattice-stability estimation methods, the minimum d^{ther}_c is given by the Tolman equation and

Table 3
Calculated d_c^{ther} values (in [nm]).

	Method I	Method II	Method III
Tolman equation	0.20 ± 0.05	0.22 ± 0.05	3.8 ± 0.4
Vogelsberger equation	0.60 ± 0.05	0.62 ± 0.05	4.2 ± 0.4
Recommended values	0.4 ± 0.2	0.4 ± 0.2	4.0 ± 0.5

the maximum by the Vogelsberger equation.

In Table 3 the average d_c^{ther} corresponding to estimation methods I to III ("recommended values") are also presented, to be compared with the experimental $d_{min} = (9 \pm 1)\ nm$. Evidently the three estimation methods yield d_c^{ther} values in agreement with eq. (1). Methods I and II lead to essentially the same value, which represents the lowest predicted d_c^{ther} whereas Method III, based on the work by Loeff, Weeber and Miedema represents the largest predicted critical diameter.

The previous comparisons suggest that the present predictive Gibbs energy approach to the amorphous/crystal phase stability leads to predicted critical diameters for a stable γ-Cu-Zn crystalline particle, which are correctly related to the experimental d_{min}.

The key contribution of the present work is to study, using detailed d_c^{ther} predictions, the effects of the uncertainty in various parameters involved in the predictive formalism which are not directly available from experiments. Specifically, various methods have been proposed and tested to determine the "lattice-stability" and the surface Gibbs energy parameter of the amorphous phase.

In particular, the present study has provided two well defined bounds to the thermodynamic stability of the amorphous phase. The lower bound corresponds to the treatment of the amorphous as an undercooled liquid phase, and the upper bound to the consideration of possible relaxation of the amorphous towards the crystalline state as suggested by Loeff, Weeber and Miedema.

Moreover, as a part of the extensive analysis of experimental data performed in the current study, various quantities have been identified which deserve further investigation. In particular, the surface contribution to the Gibbs energy of the crystalline and the amorphous phase of the present alloys should be measured. In addition, new experimental determinations of the enthalpy difference between the crystal and the amorphous, would be valuable to reduce the range of "lattice-stability" estimates for the latter phase.

Acknowledgements

This work was supported by the ANPCyT, CONICET, CNEA and Universidad Nacional de Cuyo, Argentina. Dr. Francisco Lovey is gratefully acknowledged for useful suggestions concerning the high-resolution TEM work. We also thank F. Sesma for the X-ray diffraction pattern.

References

[1] H.J. Fecht, E. Hellstern, Z. Fu, W.L. Johnson, Metall. Trans. A 21 (1990) 2333–2337.
[2] H.Y. Bai, C. Michaelsen, C. Gente, R. Bormann, Phys. Rev. B 63 (2001) 1–9.
[3] G.-P. Zheng, M. Li, Acta Mater 55 (2007) 5464–5472.
[4] R.B. Schwarz, C.C. Koch, Appl. Phys. Lett. 49 (1986) 146–148.
[5] L. Kaufman, H. Bernstein, Computer Calculation of Phase Diagrams, Academic Press, New York, 1970.
[6] H.L. Lukas, S.G. Fries, B. Sundman, Computational Thermodynamics. The Calphad Method, Cambridge University Press, New York, 2007.
[7] A.T. Dinsdale, Calphad 15 (1991) 317–425.
[8] P.I. Loeff, A.W. Weeber, A.R. Miedema, J. Less-Common Met. 140 (1988) 299–305.
[9] F.R. de Boer, R. Boom, W.C.M. Mattens, A.R. Miedema, A.K. Niessen, Cohesion in Metals, North-Holland Physics Publishing, Amsterdam, 1988.
[10] N. Das, J. Mittra, B.S. Murty, S.K. Pabi, U.D. Kulkarni, G.K. Dey, J. Alloy. Compd. 550 (2013) 483–495.
[11] C. Aguilar, P. Guzman, S. Lascano, C. Parra, L. Bejar, A. Medina, D. Guzman, J. Alloy. Compd. 670 (2016) 346–355.
[12] S. Guo, Q. Hu, C. Ng, C.T. Liu, Intermetallics 41 (2013) 96–103.
[13] Y.Y. Wang, J.H. Li, T.L. Wang, B.X. Liu, Intermetallics 53 (2014) 102–106.
[14] K.S.N. Satish Idury, B.S. Murty, J. Bhatt, Intermetallics 65 (2015) 42–50.
[15] J. Basu, B.S. Murty, S. Ranganathan, J. Alloy. Compd. 465 (2008) 163–172.
[16] A.W. Weeber, J. Phys. F. Met. Phys. 17 (1987) 809–813.
[17] M.G. Poletti, L. Battezzati, Acta Mater 75 (2014) 297–306.
[18] D.J.M. King, S.C. Middleburgh, A.G. McGregor, M.B. Cortie, Acta Mater 104 (2016) 172–179.
[19] A.K. Singh, N. Kumar, A. Dwivedi, A. Subramaniam, Intermetallics 53 (2014) 112–119.
[20] F.A. Mohamed, Acta Mater 51 (2003) 4107–4119.
[21] T. Massalski, H. Okamoto, P. Subramanian, L. Kacprzak (Eds.), Binary Alloy Phase Diagrams, second ed., American Society for Metals, Metals Park, Ohio, 1990.
[22] B.T. McDermott, C.C. Koch, Scr. Metall. 20 (1986) 669–672.
[23] F. Cardellini, V. Contini, G. Mazzone, M. Vittori, Scr. Metall. Mater 28 (1993) 1035–1038.
[24] S.K. Pabi, B.S. Murty, Mater. Sci. Eng. A 214 (1996) 146–152.
[25] S.K. Pabi, J. Joardar, B.S. Murty, J. Mater. Sci. 31 (1996) 3207–3211.
[26] S.K. Pabi, J. Joardar, I. Manna, B.S. Murty, Nanostruct. Mater 9 (1997) 149–152.
[27] J. Andrade-Gamboa, F.C. Gennari, P. Arneodo Larochette, C. Neyertz, M. Ahlers, J.L. Pelegrina, Mater. Sci. Eng. A 447 (2007) 324–331.
[28] N.K. Mukhopadhyay, D. Mukherjee, S. Bera, I. Manna, R. Manna, Mater. Sci. Eng. A 485 (2008) 673–680.
[29] H. Yang, H. Bakker, J. Alloy. Compd. 189 (1992) 113–116.
[30] J.M. López, J.A. Alonso, L.J. Gallego, Phys. Rev. B 36 (1987) 3716–3722.
[31] Z.-W. Zhang, J.-E. Zhou, S.-Q. Xi, G. Ran, P.-L. Li, W.-X. Zhang, J. Alloy. Compd. 370 (2004) 186–191.
[32] A.K. Niessen, A.R. Miedema, Ber. Bunsen Ges. Phys. Chem. 87 (1983) 717–725.
[33] A.R. Miedema, P.F. de Châtel, F.R. de Boer, Phys. B 100 (1980) 1–28.
[34] M. Ahlers, Prog. Mater. Sci. 30 (1986) 135–186.
[35] P. Wallbrecht, F. Balck, R. Blachnik, K.C. Mills, Scr. Metall. 10 (1976) 579–584.
[36] E.A. Brandes, G.B. Brook (Eds.), Smithells Metals Reference Book, seventh ed., Butterworth-Heinemann, Oxford, 1992.
[37] M.W. Chase Jr., C.A. Davies, J.R. Downey Jr., D.J. Frurip, R.A. McDonald, A.N. Syverud, JANAF thermochemical tables, third ed. J. Phys. Chem. Ref. Data 14 (Suppl. 1) (1985).
[38] G. Kaptay, J. Mater. Sci. 47 (2012) 8320–8335.
[39] G. Kaptay, J. Nanosci. Nanotech. 12 (2012) 2625–2633.
[40] V.M. Fokin, E.D. Zanotto, J. Non-Cryst. Solids 265 (2000) 105–112.
[41] F.C. Lovey, G. van Tendeloo, J. van Landuyt, M. Chandrasekaran, S. Amelinckx, Acta Metall. 32 (1984) 879–886.
[42] A. Fernández Guillermet, M. Hillert, Calphad 12 (1988) 337–349.
[43] A.R. Miedema, Z. Met. 69 (1978) 287–292.
[44] G. Kaptay, Langmuir 31 (2015) 5796–5804.
[45] J. Brillo, I. Egry, J. Mater. Sci. 40 (2005) 2213–2216.
[46] J. Brillo, G. Kolland, J. Mater. Sci. 51 (2016) 4888–4901.
[47] R. Benedictus, A. Böttger, E.J. Mittemeijer, Phys. Rev. B 54 (1996) 9109–9125.
[48] C. Li, Y.L. Chin, P. Wu, Intermetallics 12 (2004) 103–109.
[49] D. Chatain, Annu. Rev. Mater. Res. 38 (2008) 45–70.